

Bayesian Tensor Learning for Structural Monitoring Data Imputation and Response Forecasting

Pu Ren^a, Hao Sun^{a,b,*}

^a*Department of Civil and Environmental Engineering, Northeastern University, Boston, MA 02115, USA*

^b*Department of Civil and Environmental Engineering, MIT, Cambridge, MA 02139, USA*

Abstract

There has been increased interest in missing sensor data imputation, which is ubiquitous in the field of structural health monitoring (SHM) due to discontinuous sensing caused by sensor malfunction. To address this fundamental issue, this paper presents a Bayesian tensor learning method for reconstruction of spatiotemporal missing data in SHM and forecasting of structural response. In particular, a spatiotemporal tensor is first constructed followed by Bayesian tensor factorization that extracts latent features for missing data imputation. To enable structural response forecasting based on incomplete sensing data, the tensor decomposition is further integrated with vector autoregression. The performance of the proposed approach is validated on continuous field-sensing data (including strain and temperature records) of a concrete bridge, based on the assumption that strain time histories are highly correlated to temperature recordings. The results indicate that the proposed probabilistic tensor learning approach is accurate and robust even in the presence of large rates of random missing, structured missing and their combination. The effect of rank selection on the imputation and prediction performance is also investigated. The results show that a better estimation accuracy can be achieved with a higher rank for random missing whereas a lower rank for structured missing.

Keywords: Tensor decomposition, Bayesian inference, Machine learning, Data imputation, Response forecasting, Structural health monitoring

1. Introduction

High-quality data plays a pivotal role in structural health monitoring (SHM) for condition assessment, damage detection, and decision making. However, during long-term monitoring, it is inevitable for imperfect and corrupted sensor measurements, especially in a harsh and noisy environment, which calls for effective approaches for imputation/recovery missing and noisy data. Furthermore, in order to conduct real-time early-warning of structural deterioration or even disastrous failure, forecasting/prediction of structural response has also received considerable attention. The general idea of time series analysis, in the context of imputation and forecasting, is to find key dynamic patterns from observations and establish a mapping function between the historical records and the estimation. Nevertheless, these tasks are rather challenging on account of complex spatiotemporal dependencies and inherent difficulty in large-scale and nonlinear characteristics of SHM data, especially in piratical applications.

There have been a number of attempts made to solve the data imputation and forecasting problems in the SHM community. On one hand, in the missing data recovery research, compressive sensing is one common and typical approach to rebuild the entire temporal signals based on the

*Corresponding author. Tel: +1 617-373-3888

Email addresses: ren.pu@northeastern.edu (Pu Ren), h.sun@northeastern.edu (Hao Sun)

the sparsity assumption of the data in certain feature spaces [1–5]. Another interesting stream for data imputation is the use of probability methods (e.g., Gaussian process (GP) thanks to its great interpretation capacity for nonlinear dynamic processes), which has been comprehensively studied in outlier detection [6, 7], model calibration/updating [8–14] and system identification [15–20]. For instance, Wan *et al.* [21] employed Bayesian multi-task learning with multi-dimensional GP priors to recover SHM data. Chen *et al.* [22] explored the possibility of probability density function estimation for data loss compensation with warping transformations. Some recent surveys have reported the great potential in data imputation by considering both the sensor information and time series, which is usually conceptualized as spatiotemporal. Yang *et al.* [23] developed a low-rank matrix completion method with ℓ_1 -norm and a nuclear norm for imputation of random missing data. This approach is powerful but has limitations due to an ideal assumption that the data is randomly missing, which is less common in practical SHM (e.g., data might be missing for a continuous duration). Chen *et al.* [24] investigated the inter-sensor relationship of stochastic structural responses with non-parametric copulas, which flexibly captured the spatial dependency for strain data. Moreover, the sequential broad learning (SBL) approach was recently presented for efficiently reconstructing structural response [25], which is however short for spatial consideration. On the other hand, for the sake of data-driven structural response forecasting, the majority of existing research focus on the time-dependent response approximation based on high-quality collected data (e.g., data missing is not considered). In particular, the widely-accepted and well-studied methods are based on the linear combination of previous observations, for example, dynamic linear models [26–28] and autoregressive (AR) models [29–31]. Distinctively, Wan and Ni [32] examined the capability of a GP-based Bayesian approach for underlying nonlinear dynamic system response prediction from a statistic perspective. Besides, deep learning techniques, such as the convolutional neural network (CNN) [33–35], the long-short term memory (LSTM) network [36, 37], and the variational autoencoder (VAE) [38], have also been proven to be a decent alternative for extracting spatial features for dynamic response reconstruction and prediction.

Despite the rapid development of data science in SHM, there still remain three representative challenges for the specific aim of data imputation and response forecasting. Firstly, very little work has been devoted to the spatial dependency and correlation in the time series analysis. The second is the lack of consideration on vast and continuous missing scenarios (e.g., data missing for a long continuous period such as one day or consecutive days). Lastly, almost all of the present studies on response forecasting are based on high-quality data instead of imperfect measurements with missing values. To this end, in light of the recent renaissance in tensor learning [39–41], which has already greatly contributed to image processing [42–47], recommender systems [48–50], and traffic data analysis [51–59], we propose a Bayesian tensor learning method for (1) reconstruction of spatiotemporal missing data in SHM and (2) forecasting of structural response under the scenario of missing/incomplete data. Different from [23], tensor factorization in the context of Bayesian inference provides a principled selection mechanism for suitable likelihood models and allows for uncertainty quantification in parameter estimation and prediction [60]. In addition, inspired by the strong correlation between strain data and temperature data [28, 61–64], this research sheds new light on integrating physics into the tensor model, resulting in an interpretative low-rank data structure.

The main contribution of this paper can be summarized as follows. Firstly, to the best of our knowledge, it is the first time to realize response forecasting with incomplete data in SHM applications, based on reliable latent features instead of directly using the corrupted data. Secondly, by constructing one-dimensional time series data into a second-order tensor structure (sensor locations \times time steps), we can easily capture the spatiotemporal features of the data for accurate imputation and forecasting. Thirdly, the physics relationship between strain and temperature is introduced

to optimize the tensor structure. We further validate the proposed approach on a concrete bridge with multi-year recordings of strain and temperature time histories.

The rest of the paper is organized as follows, in addition to this Introduction section. Section 2 begins by laying out the theoretical dimensions of this work, and is concerned with the proposed methodology. In Section 2.1, we describe the problem definition and general principle of data imputation and response forecasting under the data missing scenarios. In Section 2.2, 2.3 and 2.4, we circumstantially present the Bayesian generation and inference procedure, as well as the autoregressive process for temporal feature modeling. Section 3 elaborates the experimental validation results of the proposed method, focusing on three key themes: imputation and forecasting performance with respect to different missing rates, uncertainty quantification and rank analysis. Section 4 concludes the current work and the outlook of future directions.

2. Methodology

In this section, we formulate the problem of SHM data imputation and response forecasting in the context of tensor learning, and present the spatiotemporal dependency modeling procedure via matrix factorization.

2.1. Problem Description

The goal of SHM data imputation and forecasting is to estimate the missing values and predict the future structural response given partially observed data collected from a sensor network. The multidimensional time series data, with missing values, can be represented by matrix $\mathbf{Y} \in \mathbb{R}^{M \times T}$, where M denotes the number of sensor locations and T is the number of time stamps for a certain continuously monitoring period. The imputation process aims to firstly learn a factorized spatial feature \mathbf{U} and a temporal feature \mathbf{X} based on the observed data \mathbf{Y} , and then reconstruct the response with imputed values. Afterwards, given $\mathbf{y}_{:,t}$ signifying the multivariate data at time t , the course of response forecasting utilizes the well-trained spatial factor \mathbf{U} and the updated temporal factor \mathbf{X}^* to map $L (\geq 1)$ historical sensing data to future $\mathcal{T} (\geq 1)$ structural responses, given by

$$[\mathbf{y}_{:,t-L+1}, \dots, \mathbf{y}_{:,t}] \xrightarrow[\mathbf{X}^*]{\mathbf{U}} [\mathbf{y}_{:,t+1}, \dots, \mathbf{y}_{:,t+\mathcal{T}}] \quad (1)$$

which essentially establishes a temporal forecasting process.

2.2. Model Generation

Naturally, spatiotemporal SHM data observed from M sensor locations with T time stamps can be constructed in the form of a two-dimensional tensor, $\mathbf{Y} \in \mathbb{R}^{M \times T}$. Due to inevitable data missing in practical applications, we define an indicator set for the observed elements in \mathbf{Y} as $\Omega = \{(i, t) | y_{i,t} \text{ is observed}\}$. To characterize the spatiotemporal dependencies, we employ the general idea of second-order tensor (matrix) decomposition to approximate the multidimensional data through the sum of K rank-1 tensors, namely,

$$\mathbf{Y} \approx \sum_{r=1}^K \mathbf{u}_r \circ \mathbf{x}_r = \mathbf{U}^\top \mathbf{X}, \quad (2)$$

where K is a positive integer referring to the tensor rank, and the symbol \circ stands for the vector outer product. Here, $\mathbf{u}_1, \mathbf{u}_2, \dots, \mathbf{u}_K \in \mathbb{R}^M$ and $\mathbf{x}_1, \mathbf{x}_2, \dots, \mathbf{x}_K \in \mathbb{R}^T$ form the rank-1 components of the matrix \mathbf{Y} . Furthermore, with this formulation, we assume \mathbf{U} as the spatial latent factor whose rows are \mathbf{u}_r 's, and \mathbf{X} to be the temporal latent feature whose rows are \mathbf{x}_r 's. Element-wise, $y_{i,t}$ is

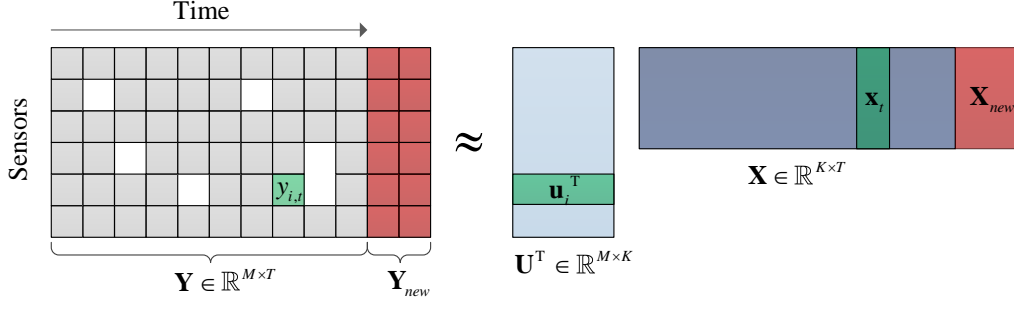


Figure 1: A graphic illustration of matrix factorization. Note that the white boxes represent the missing values while the grey boxes denote the observed data.

estimated by the inner product of \mathbf{u}_i and \mathbf{x}_t , where $\mathbf{u}_i \in \mathbb{R}^K$ represents the latent spatial feature at sensor i and $\mathbf{x}_t \in \mathbb{R}^K$ is the latent temporal embedding at time t , expressed as

$$y_{i,t} \approx \mathbf{u}_i^\top \mathbf{x}_t. \quad (3)$$

The basic concept of matrix factorization is illustrated in Figure 1.

Next, we present the fully Bayesian method for tensor learning. To begin this process, the likelihood of the observed SHM data $y_{i,t}$ is given by:

$$y_{i,t} \sim \mathcal{N}(\mathbf{u}_i^\top \mathbf{x}_t, \tau_\epsilon^{-1}), \quad (4)$$

where $\mathcal{N}(\cdot)$ denotes the Gaussian distribution with mean $\mathbf{u}_i^\top \mathbf{x}_t$ and precision τ_ϵ . Secondly, to model the spatial factor, the prior distribution over the spatial feature vectors (i.e., \mathbf{u}_i) is assumed to be multivariate Gaussian, viz.,

$$\mathbf{u}_i \sim \mathcal{N}(\boldsymbol{\mu}_u, \boldsymbol{\Lambda}_u^{-1}). \quad (5)$$

We further place conjugate Gaussian-Wishart priors on the spatial feature parameters $\boldsymbol{\Theta}_u = \{\boldsymbol{\mu}_u, \boldsymbol{\Lambda}_u\}$, i.e., mean $\boldsymbol{\mu}_u \in \mathbb{R}^K$ and variance $\boldsymbol{\Lambda}_u \in \mathbb{R}^{K \times K}$, written as

$$\begin{aligned} p(\boldsymbol{\Theta}_u | \boldsymbol{\mu}_0, \beta_0, \mathbf{W}_0, v_0) &= p(\boldsymbol{\mu}_u | \boldsymbol{\Lambda}_u) p(\boldsymbol{\Lambda}_u) \\ &= \mathcal{N}(\boldsymbol{\mu}_u | \boldsymbol{\mu}_0, (\beta_0 \boldsymbol{\Lambda}_u)^{-1}) \mathcal{W}(\boldsymbol{\Lambda}_u | \mathbf{W}_0, v_0). \end{aligned} \quad (6)$$

Here, $\boldsymbol{\mu}_0, \beta_0, \mathbf{W}_0, v_0$ are hyper-parameters; $\mathcal{W}(\cdot)$ denotes the Wishart distribution with v_0 degrees of freedom and a $K \times K$ scale matrix \mathbf{W}_0 , namely,

$$\mathcal{W}(\boldsymbol{\Lambda}_u | \mathbf{W}_0, v_0) = \frac{1}{C} |\boldsymbol{\Lambda}_u|^{\frac{v_0 - K - 1}{2}} \exp\left(-\frac{1}{2} \text{Tr}(\mathbf{W}_0^{-1} \boldsymbol{\Lambda}_u)\right), \quad (7)$$

where C is the normalizing constant and $\text{Tr}(\cdot)$ denotes the matrix trace defined as the sum of all the elements on the main diagonal of the matrix.

Although probabilistic modeling of the spatial factors is straightforward, it is tricky to capture the time-evolving patterns and predict the dynamic trends in the Bayesian learning. Here, we consider incorporating the AR process into the matrix/tensor factorization model for describing the temporal dependencies. Generally, an AR model is characterized by a time lag set and a weight parameter vector. However, different from the traditional AR model which is more applicable for low-dimensional data, we make two modifications to handle the multi-dimensional time-series issue. The first distinction is that we introduce a flexible AR structure on time lags \mathcal{L} [51]. Instead of

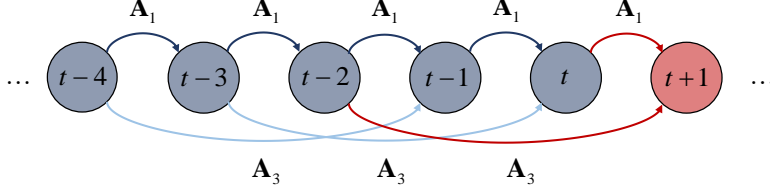


Figure 2: Auto-regressive model for temporal dependencies.

applying a small-size lag set (e.g., $\mathcal{L} = \{1\}$) which only learns the simple temporal patterns (e.g., daily similarity), we try to use more complex time lags to infer seasonal or yearly trends for long-term forecasting. The second alteration is changing the tensor structure of AR model parameters for convenience. Let the time lags set be $\mathcal{L} = \{l_1, l_2, \dots, l_d\}$, where d is the order of the AR model. In our case, the weight parameter \mathbf{A}_j ($j \in \{1, 2, \dots, d\}$) should be a $K \times K$ matrix since the elements in the AR model are formed as column vectors (i.e., $\mathbf{x}_t \in \mathbb{R}^{K \times 1}$) in the temporal feature matrix \mathbf{X} . The graphic illustration is shown in Figure 2 with the example of $\mathcal{L} = \{1, 3\}$.

In addition, there is no diagonal restriction on \mathbf{A}_j due to the complicated causal relationship between factors. Thus, the reorganized formulation of the AR process can be written as:

$$\begin{aligned} \mathbf{x}_{t+1} &\approx \mathbf{A}_1 \mathbf{x}_{t+1-l_1} + \mathbf{A}_2 \mathbf{x}_{t+1-l_2} + \dots + \mathbf{A}_d \mathbf{x}_{t+1-l_d} \\ &= \underbrace{[\mathbf{A}_1, \mathbf{A}_2, \dots, \mathbf{A}_d]}_{\mathbf{A}} \underbrace{[\mathbf{x}_{t+1-l_1}, \mathbf{x}_{t+1-l_2}, \dots, \mathbf{x}_{t+1-l_d}]}_{\mathbf{z}_{t+1}}^\top. \end{aligned} \quad (8)$$

For simplicity, we define a time-invariant matrix $\mathbf{A} \in \mathbb{R}^{(Kd) \times K}$ and a historical observation vector $\mathbf{z}_{t+1} \in \mathbb{R}^{(Kd) \times 1}$ shown in Eq. (8). As a result, by assuming the prior distribution for the temporal factor \mathbf{x}_t as multivariate Gaussian, we have the mean vector as $\mathbf{A}^\top \mathbf{z}_t$ for the forecasting process. Therefore, the piecewise modeling of the temporal feature matrix is summarized as:

$$\begin{aligned} \mathbf{x}_t &\sim \mathcal{N}(\tilde{\boldsymbol{\mu}}_x, \tilde{\boldsymbol{\Sigma}}_x) \\ &\sim \begin{cases} \mathcal{N}(\mathbf{0}, \mathbf{I}_x), & \text{if } t \in \{1, 2, \dots, l_d\}, \\ \mathcal{N}(\mathbf{A}^\top \mathbf{z}_t, \boldsymbol{\Sigma}), & \text{otherwise,} \end{cases} \end{aligned} \quad (9)$$

where $\mathbf{0} \in \mathbb{R}^{K \times 1}$ is a zero vector and $\mathbf{I}_x \in \mathbb{R}^{K \times K}$ is an identity matrix.

Likewise, a conjugate Matrix Normal Inverse Wishart prior is applied to the hyper-parameters $\boldsymbol{\Theta}_x = \{\mathbf{A}, \boldsymbol{\Sigma}\}$ in the forecasting process:

$$\begin{aligned} p(\boldsymbol{\Theta}_x | \mathbf{A}_0, \mathbf{V}_0, \boldsymbol{\Psi}_0, v_0) &= p(\mathbf{A} | \boldsymbol{\Sigma}) p(\boldsymbol{\Sigma}) \\ &= \mathcal{MN}(\mathbf{A} | \mathbf{A}_0, \mathbf{V}_0, \boldsymbol{\Sigma}) \mathcal{IW}(\boldsymbol{\Sigma} | \boldsymbol{\Psi}_0, v_0), \end{aligned} \quad (10)$$

where $\mathcal{MN}(\cdot)$ is Matrix Normal distribution and $\mathcal{IW}(\cdot)$ denotes Inverse Wishart function. Herein, the Inverse-Wishart distribution $\boldsymbol{\Sigma} \sim \mathcal{IW}(\boldsymbol{\Psi}_0, v_0)$ is equivalent to $\boldsymbol{\Sigma}^{-1} \sim \mathcal{W}(\boldsymbol{\Psi}_0^{-1}, v_0)$. Besides, the probability density function (PDF) for \mathbf{A} is given by

$$p(\mathbf{A} | \mathbf{A}_0, \mathbf{V}_0, \boldsymbol{\Sigma}) = (2\pi)^{-\frac{K^2 d}{2}} |\mathbf{V}_0|^{-\frac{K}{2}} |\boldsymbol{\Sigma}|^{-\frac{Kd}{2}} \exp^{-\frac{1}{2} [\text{Tr}(\boldsymbol{\Sigma}^{-1} (\mathbf{A} - \mathbf{A}_0)^\top \mathbf{V}_0 (\mathbf{A} - \mathbf{A}_0))]} \quad (11)$$

in which $\mathbf{A}_0 \in \mathbb{R}^{(Kd) \times K}$ is the mean matrix parameter, $\mathbf{V}_0 \in \mathbb{R}^{(Kd) \times (Kd)}$ represents the row-variance matrix, and $\boldsymbol{\Sigma} \in \mathbb{R}^{K \times K}$ denotes the column-variance matrix parameter.

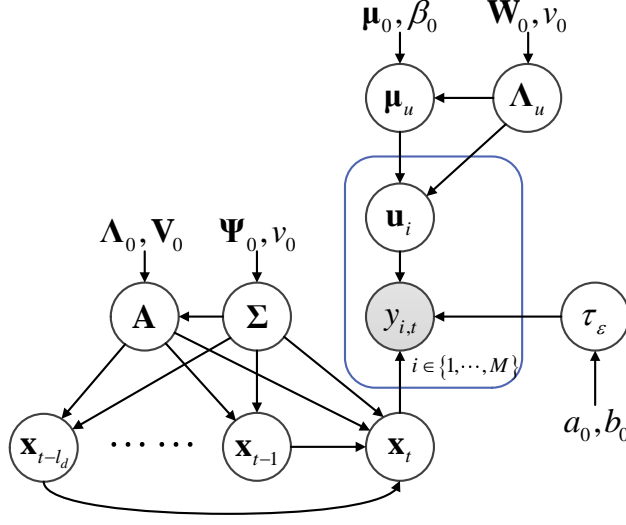


Figure 3: Probabilistic graphic model for Bayesian tensor learning.

The final stage of model generation is to deal with the precision parameter τ_ϵ as shown in Eq. (4). In particular, a conjugate Gamma prior over τ_ϵ is introduced to make the generative model robust in consideration of the indeterminate noise effect in SHM data:

$$\tau_\epsilon \sim \text{Gamma}(a_0, b_0) \quad (12)$$

Here we define $\Theta_\tau = \{a_0, b_0\}$ where a_0 and b_0 represent the shape parameter and the rate parameter, respectively. The PDF of τ_ϵ has the form as follows

$$p(\tau_\epsilon | a_0, b_0) = \frac{b_0^{a_0}}{\Gamma(a_0)} \tau_\epsilon^{a_0-1} \exp(-b_0 \tau_\epsilon). \quad (13)$$

The graphic model representing the generative Bayesian tensor learning described above is depicted in Figure 3. The grey node $y_{i,t}$ ($(i, t) \in \Omega$) is the observed SHM data, while \mathbf{u}_i , \mathbf{x}_t and τ_ϵ are the parameters in the likelihood distribution 4. In our experiments, we initialize the scalars as: $\beta_0 = 1, v_0 = K, a_0 = b_0 = 1 \times 10^{-6}$. The vector μ_0 and the matrix Λ_0 are set as a zeros. The remaining matrices $\{\mathbf{W}_0, \mathbf{V}_0, \Psi_0\}$ are all set to be identity matrix but with different dimensions.

2.3. Model Inference

Following the Bayesian modeling formulation in [42] and [65], we infer the predictive distribution over missing entries below:

$$p(y_{i,t}^* | \mathbf{Y}, \Theta_0^u, \Theta_0^x) = \iint p(y_{i,t}^* | \mathbf{u}_i, \mathbf{x}_t, \tau_\epsilon) p(\mathbf{U}, \mathbf{X}, \tau_\epsilon | \mathbf{Y}, \Theta_u, \Theta_x, \Theta_\tau) p(\Theta_u, \Theta_x, \Theta_\tau | \Theta_0^u, \Theta_0^x) d\{\mathbf{U}, \mathbf{X}, \tau_\epsilon\} d\{\Theta_u, \Theta_x, \Theta_\tau\} \quad (14)$$

where $\Theta_0^u = \{\mu_0, \beta_0, \mathbf{W}_0, v_0\}$ and $\Theta_0^x = \{\Lambda_0, \mathbf{V}_0, \Psi_0, v_0\}$ are assemblies of the hyper-parameters. Noteworthy, the exact solution of Eq. (14) cannot be obtained analytically due to the intricate integration over all the latent variables and hyper-parameters. Therefore, we seek to use Markov Chain Monte Carlo (MCMC) sampling [66] to approximate the inference. The underlying logic of

MCMC sampling is that we can draw dependent sequences of samples representing the posterior distribution. Thus, we can describe the predictive distribution in Eq. (14) as:

$$p(y_{i,t}^* | \mathbf{Y}, \boldsymbol{\Theta}_0^u, \boldsymbol{\Theta}_0^x) \approx \frac{1}{N} \sum_{n=1}^N p\left(y_{i,t}^* | \mathbf{u}_i^{(n)}, \mathbf{x}_t^{(n)}, \tau_\epsilon^{(n)}\right), \quad (15)$$

where $\{\mathbf{u}_i^{(n)}, \mathbf{x}_t^{(n)}, \tau_\epsilon^{(n)}\}$ denote the n^{th} simulated sample from the posterior distribution of interest. Herein, we introduce the Gibbs sampling [67] to generate the posterior samples, which is a sequential sampling approach by sweeping through each variable to sample from its conditional distribution with the remaining variables fixed to their current values. In addition, thanks to the use of conjugate priors in the Bayesian model generation, we can easily derive the conditional distributions since the posterior distribution is in the same probability distribution family as the prior distribution. The Gibbs sampling procedure for all the parameters and hyper-parameters are described below.

2.3.1. Sampling Spatial Features

We sample the spatial hyper-parameters $\boldsymbol{\Theta}_u$ first. Considering the likelihood in Eq. (5) and the prior in Eq. (6), the posterior distribution is given by a Gaussian-Wishart distribution:

$$\begin{aligned} p(\boldsymbol{\mu}_u, \boldsymbol{\Lambda}_u | \mathbf{U}, \boldsymbol{\Theta}_0^u) &= \mathcal{N}(\boldsymbol{\mu}_u | \boldsymbol{\mu}_0^*, (\beta_0^* \boldsymbol{\Lambda}_u)^{-1}) \mathcal{W}(\boldsymbol{\Lambda}_u | \mathbf{W}_0^*, v_0^*) \\ &\propto \prod_{i=1}^M \mathcal{N}(\mathbf{u}_i | \boldsymbol{\mu}_u, \boldsymbol{\Lambda}_u^{-1}) \times \mathcal{N}(\boldsymbol{\mu}_u | \boldsymbol{\mu}_0, (\beta_0 \boldsymbol{\Lambda}_u)^{-1}) \times \mathcal{W}(\boldsymbol{\Lambda}_u | \mathbf{W}_0, v_0) \end{aligned} \quad (16)$$

where

$$\begin{aligned} \boldsymbol{\mu}_0^* &= \frac{\beta_0 \boldsymbol{\mu}_0 + M \bar{\mathbf{u}}}{\beta_0 + M}, \quad \beta_0^* = \beta_0 + M, \quad v_0^* = v_0 + M, \\ (\mathbf{W}_0^*)^{-1} &= \mathbf{W}_0^{-1} + M \bar{\mathbf{S}} + \frac{\beta_0 M}{\beta_0 + M} (\boldsymbol{\mu}_0 - \bar{\mathbf{u}})(\boldsymbol{\mu}_0 - \bar{\mathbf{u}})^\top. \end{aligned} \quad (17)$$

Here, $\bar{\mathbf{u}}$ and $\bar{\mathbf{S}}$ are two statistical parameters defined as:

$$\bar{\mathbf{u}} = \frac{1}{M} \sum_{i=1}^M \mathbf{u}_i, \quad \bar{\mathbf{S}} = \frac{1}{M} \sum_{i=1}^M (\mathbf{u}_i - \bar{\mathbf{u}})(\mathbf{u}_i - \bar{\mathbf{u}})^\top. \quad (18)$$

The conditional distribution over spatial features \mathbf{u}_i , conditioned on temporal features \mathbf{X} , partially observed sensor data \mathbf{Y} , precision τ_ϵ and all other hyper-parameters of interest can then be obtained:

$$\begin{aligned} p(\mathbf{u}_i | \mathbf{Y}, \mathbf{X}, \boldsymbol{\Theta}_u, \tau_\epsilon) &= \mathcal{N}(\mathbf{u}_i | \boldsymbol{\mu}_u^*, (\boldsymbol{\Lambda}_u^*)^{-1}) \\ &\propto \prod_{t=1}^T \mathcal{N}(y_{i,t} | \mathbf{u}_i^\top \mathbf{x}_t, \tau_\epsilon) \times \mathcal{N}(\mathbf{u}_i | \boldsymbol{\mu}_u, (\boldsymbol{\Lambda}_u)^{-1}), \end{aligned} \quad (19)$$

where

$$\begin{aligned} \boldsymbol{\Lambda}_u^* &= \boldsymbol{\Lambda}_u + \tau_\epsilon \sum_{t=1}^T \mathbf{x}_t \mathbf{x}_t^\top, \\ \boldsymbol{\mu}_u^* &= (\boldsymbol{\Lambda}_u^*)^{-1} \left(\tau_\epsilon \sum_{i=1}^T \mathbf{x}_i y_{i,t} + \boldsymbol{\Lambda}_u \boldsymbol{\mu}_u \right), \quad (i, t) \in \Omega. \end{aligned} \quad (20)$$

2.3.2. Sampling Temporal Features

Following the sampling procedure for spatial features, we infer the conditional distribution of the hyper-parameters Θ_x with the likelihood in Eq. (9) and the prior in Eq. (10), namely,

$$\begin{aligned} p(\mathbf{A}, \Sigma | \mathbf{X}, \Theta_0^x) &= \mathcal{MN}(\mathbf{A} | \Lambda_0^*, \mathbf{V}_0^*, \Sigma) \mathcal{IW}(\Sigma | \Psi_0^*, v_0^*) \\ &\propto \prod_{t=1}^T \mathcal{N}(\mathbf{x}_t | \tilde{\mu}_x, \tilde{\Sigma}_x) \times \mathcal{MN}(\mathbf{A} | \Lambda_0, \mathbf{V}_0, \Sigma) \times \mathcal{IW}(\Sigma | \Psi_0, v_0). \end{aligned} \quad (21)$$

Matching the coefficients of the hyper-parameters in Eq. (21), we can obtain the updated parameters as follows:

$$\begin{aligned} \mathbf{V}_0^* &= (\mathbf{V}_0^{-1} + \mathbf{Q}^\top \mathbf{Q})^{-1}, \\ \Lambda_0^* &= \mathbf{V}_0^* (\mathbf{V}_0^{-1} \Lambda_0 + \mathbf{Q}^\top \mathbf{P}), \\ v_0^* &= v_0 + T - l_d, \\ \Psi_0^* &= \Psi_0 + \mathbf{P}^\top \mathbf{P} + \Lambda_0^\top \mathbf{V}_0^{-1} \Lambda_0 - (\Lambda_0^*)^\top (\mathbf{V}_0^*)^{-1} \Lambda_0^*. \end{aligned} \quad (22)$$

These two matrices $\mathbf{P} \in \mathbb{R}^{(T-l_d) \times K}$ and $\mathbf{Q} \in \mathbb{R}^{(T-d) \times (Kd)}$ are defined for simplicity and convenience, expressed as

$$\begin{aligned} \mathbf{P} &= [\mathbf{x}_{l_d+1}^\top, \dots, \mathbf{x}_T^\top]^\top, \\ \mathbf{Q} &= [\mathbf{z}_{l_d+1}^\top, \dots, \mathbf{z}_T^\top]^\top. \end{aligned} \quad (23)$$

After sampling the hyper-parameters, we further derive the conditional distribution of the temporal factor \mathbf{x}_t , whose posterior distribution follows Gaussian, given by

$$\begin{aligned} p(\mathbf{x}_t | \mathbf{Y}, \mathbf{U}, \Theta_x, \tau_\epsilon) &= \mathcal{N}(\mathbf{x}_t | \mu_x^*, \Sigma_x^*) \\ &\propto \prod_{i=1}^M \mathcal{N}(y_{i,t} | \mathbf{u}_i^\top \mathbf{x}_t, \tau_\epsilon) \times \mathcal{N}(\mathbf{x}_t | \tilde{\mu}_x, \tilde{\Sigma}_x). \end{aligned} \quad (24)$$

Nevertheless, sampling \mathbf{x}_t is complicated due to the piecewise Bayesian modeling on the temporal feature parameters. Here, we introduce four auxiliary variables $\{\mathbf{C}, \mathbf{D}, \mathbf{E}, \mathbf{F}\}$ considering the function of the AR process. The general updating formulation can thus be written as

$$\begin{aligned} \Sigma_x^* &= \left(\tau_\epsilon \sum_{i=1}^M \mathbf{u}_i \mathbf{u}_i^\top + \mathbf{C} + \mathbf{D} \right)^{-1}, \\ \mu_x^* &= \Sigma_x^* \left(\tau_\epsilon \sum_{i=1}^M \mathbf{u}_i y_{i,t} + \mathbf{E} + \mathbf{F} \right), \quad (i, t) \in \Omega. \end{aligned} \quad (25)$$

where the variables \mathbf{C} and \mathbf{E} are given by

$$\mathbf{C} = \begin{cases} \sum_{j=1, l_d < t+l_j \leq T}^d \mathbf{A}_j^\top \Sigma^{-1} \mathbf{A}_j, & \text{if } t \in \{1, 2, \dots, T - l_1\}, \\ \mathbf{0}, & \text{otherwise,} \end{cases} \quad (26)$$

$$\mathbf{E} = \begin{cases} \sum_{j=1, l_d < t+l_j \leq T}^d \mathbf{A}_j^\top \Sigma^{-1} \phi_{t+l_j}, & \text{if } t \in \{1, 2, \dots, T - l_1\}, \\ \mathbf{0}, & \text{otherwise,} \end{cases} \quad (27)$$

with ϕ_{t+l_j} being defined as

$$\phi_{t+l_j} = \mathbf{x}_{t+l_j} - \sum_{p=1, p \neq j}^d \mathbf{A}_p \mathbf{x}_{t+l_j-l_p}. \quad (28)$$

In addition, the variables \mathbf{D} and \mathbf{F} can be written as

$$\mathbf{D} = \begin{cases} \mathbf{I}_x, & \text{if } t \in \{1, 2, \dots, l_d\}, \\ \Sigma^{-1}, & \text{otherwise,} \end{cases} \quad (29)$$

$$\mathbf{F} = \begin{cases} \mathbf{0}, & \text{if } t \in \{1, 2, \dots, l_d\}, \\ (\Sigma^{-1}) \sum_{p=1}^d \mathbf{A}_p \mathbf{x}_{t-l_p}, & \text{otherwise.} \end{cases} \quad (30)$$

2.3.3. Sampling Precision

With the combination of the likelihood in Eq. (4) and the prior in Eq. (12), the posterior distribution of precision τ_ϵ can be represented by a Gamma distribution, namely,

$$\begin{aligned} p(\tau_\epsilon | \mathbf{Y}, \mathbf{U}, \mathbf{X}, \Theta_\tau) &= \text{Gamma}(a_0^*, b_0^*) \\ &\propto \prod_{i=1}^M \prod_{t=1}^T \mathcal{N}(y_{i,t} | \mathbf{u}_i^\top \mathbf{x}_t, \tau_\epsilon) \times \text{Gamma}(\tau_\epsilon | a_0, b_0), \end{aligned} \quad (31)$$

where the hyper-parameters a_0^* and b_0^* can be expressed as

$$\begin{aligned} a_0^* &= \frac{1}{2} \sum_{(i,t) \in \Omega} s_{i,t} + a_0, \\ b_0^* &= \frac{1}{2} \sum_{(i,t) \in \Omega} (y_{i,t} - \mathbf{u}_i^\top \mathbf{x}_t)^2 + b_0. \end{aligned} \quad (32)$$

Note that $s_{i,t}$ is 1 if $(i, t) \in \Omega$ and 0 otherwise.

2.4. Response Forecasting

As described in Figure 1, we predict the future structural response $y_{i,t+1}$ based on the learned spatial feature \mathbf{u}_i and the newly updated temporal feature \mathbf{x}_{t+1} . To be more specific, after getting well-trained parameters from the imputation process, we keep $\{\mathbf{U}, \mathbf{X}, \mathbf{A}\}$ unchanged for the forecasting step and only view $\{\Sigma, \mathbf{x}_t, \tau_\epsilon\}$ as the updated targets. Moreover, to predict $y_{i,t+2}$ sequentially, we provide the observed $y_{i,t+1}$ as an input and conduct the above procedure iteratively. The general philosophy of Bayesian forecasting can be illustrated by two steps as follows.

The first step is to learn \mathbf{x}_t from the historical observation $\mathbf{y}_{:,t}$. The model generative formulations are expressed as:

$$\begin{aligned} y_{i,t} &\sim \mathcal{N}(\mathbf{u}_i^\top \mathbf{x}_t, \tau_\epsilon^{-1}), \\ \mathbf{x}_t &\sim \mathcal{N}(\tilde{\boldsymbol{\mu}}_x, \tilde{\Sigma}_x), \\ \tilde{\Sigma}_x &\sim \mathcal{IW}(\Psi_0, v_0), \\ \tau_\epsilon &\sim \text{Gamma}(a_0, b_0) \end{aligned} \quad (33)$$

where $\tilde{\boldsymbol{\mu}}_x$ is a known parameter denoted as $\mathbf{A}^\top \mathbf{z}_t$. Note that there is possible missing values in $\mathbf{y}_{:,t}$. The model inference using Gibbs sampling for this step is divided into three parts. To begin with, we need to do sampling on the hyper-parameter $(\tilde{\Sigma}_x)^{-1} \sim \mathcal{W}((\Psi_0^*)^{-1}, v_0 + 1)$ where

$$\Psi_0^* = \Psi_0 + (\mathbf{x}_t - \mathbf{A}^\top \mathbf{z}_t)(\mathbf{x}_t - \mathbf{A}^\top \mathbf{z}_t)^\top. \quad (34)$$

Then we sample the future temporal factor $\mathbf{x}_t \sim \mathcal{N}((\tilde{\boldsymbol{\mu}}_x)^*, (\tilde{\boldsymbol{\Sigma}}_x)^*)$ with

$$\begin{aligned}\tilde{\boldsymbol{\Sigma}}_x^* &= \left(\tau_\epsilon \sum_{i=1}^M \mathbf{u}_i \mathbf{u}_i^\top + \tilde{\boldsymbol{\Sigma}}_x^{-1} \right)^{-1}, \\ \tilde{\boldsymbol{\mu}}_x^* &= \tilde{\boldsymbol{\Sigma}}_x^* \left(\tau_\epsilon \sum_{i=1}^M \mathbf{u}_i y_{i,t} + \tilde{\boldsymbol{\Sigma}}_x^{-1} \mathbf{A}^\top \mathbf{z}_t \right).\end{aligned}\tag{35}$$

The third part is the sampling of the precision parameter τ_ϵ using Eq. (32).

After generating samples of \mathbf{x}_t , the second step for forecasting is that we run Gibbs sampling on the prediction for multiple iterations based on $\mathbf{y}_{:,t+1} \approx \mathbf{U}^\top (\mathbf{A}^\top \mathbf{z}_{t+1})$, and get the average of these samples in the burn-in period as output. This is an efficient strategy for forecasting, especially for large-scale problems. The pseudo code for the proposed Bayesian tensor learning for missing SHM data imputation and structural response forecasting is summarized in Algorithm 1.

Algorithm 1: Gibbs sampling for Bayesian tensor learning

Input: the SHM data tensor \mathbf{Y} , the indicator tensor $\boldsymbol{\Omega}$, the chain length for imputation N_1^{mc} , the burn-in period for imputation N_1^{b} , the chain length for forecasting N_2^{mc} , the burn-in period for forecasting N_2^{b} , tensor rank K and time lags \mathcal{L} .

Output: the chains of samples for the estimated tensor $\hat{\mathbf{Y}}_1$ and the predicted tensor $\hat{\mathbf{Y}}_2$.

```

1 Initialize:  $\mathbf{U}$ ,  $\mathbf{X}$ ,  $\mathbf{A}$ ,  $\boldsymbol{\Theta}_0^u$ ,  $\boldsymbol{\Theta}_0^x$  and  $\boldsymbol{\Theta}_\tau$ ;
   // The imputation process
2 for  $n_1 = 1, \dots, N_1^{\text{mc}}$  do
3   | Sample the hyperparameter  $\boldsymbol{\Theta}_u$  (Eq. 16);
4   |  $\boldsymbol{\Theta}_u \sim p(\boldsymbol{\Theta}_u | \mathbf{U}, \boldsymbol{\Theta}_0^u)$ ;
5   | for  $i = 1, \dots, M$  do
6   |   | Sample spatial feature  $\mathbf{u}_i$  (Eq. 19);
7   |   |  $\mathbf{u}_i \sim p(\mathbf{u}_i | \mathbf{Y}, \mathbf{X}, \boldsymbol{\Theta}_u, \tau_\epsilon)$ ;
8   | end
9   | Sample the hyperparameter  $\boldsymbol{\Theta}_x$  (Eq. 21);
10  |  $\boldsymbol{\Theta}_x \sim p(\boldsymbol{\Theta}_x | \mathbf{X}, \boldsymbol{\Theta}_0^x)$ ;
11  | for  $t = 1, \dots, T$  do
12  |   | Sample temporal feature  $\mathbf{x}_t$  (Eq. 24);
13  |   |  $\mathbf{x}_t \sim p(\mathbf{x}_t | \mathbf{Y}, \mathbf{U}, \boldsymbol{\Theta}_x, \tau_\epsilon)$ ;
14  | end
15  | Sample the precision parameter  $\tau_\epsilon$  (Eq. 31);
16  |  $\tau_\epsilon \sim p(\tau_\epsilon | \mathbf{Y}, \mathbf{U}, \mathbf{X}, \boldsymbol{\Theta}_\tau)$ ;
17  | if  $n_1 \geq N_1^{\text{b}}$  then
18  |   | Compute and collect the sample  $\hat{\mathbf{Y}}_1 = \mathbf{U}^\top \mathbf{X}$ ;
19  | end
20 end
   // The forecasting process
21 for  $n_2 = 1, \dots, N_2^{\text{mc}}$  do
22  | Sample the hyperparameter  $\tilde{\boldsymbol{\Sigma}}_x$  (Eq. 34);
23  | Sample the temporal feature  $\mathbf{x}_t$  (Eq. 35);
24  | Sample the precision parameter  $\tau_\epsilon$  (Eq. 31);
25  | if  $n_2 \geq N_2^{\text{b}}$  then
26  |   | Compute and collect the sample  $\hat{\mathbf{Y}}_2 = \mathbf{U}^\top (\mathbf{A} \mathbf{z}_{t+1})$ ;
27  | end
28 end

```

3. Experimental Validation

In this section, we test the imputation and forecasting performance of the proposed Bayesian tensor learning method under data missing scenarios, using long-term field-monitoring data of a concrete bridge (e.g., strain and temperature records). In particular, we impute and forecast the strain time histories of the bridge. Inspired by the strong correlation between strain and temperature, we formulate the tensor data structure by combining both strain and temperature along the sensor dimension. We also conduct a series of analyses of uncertainty quantification and rank selection for tensor factorization. The numerical analyses are performed on a standard PC with 28 Intel Core i9-7940X CPUs and 2 NVIDIA GTX 1080 Ti video cards.

3.1. Bridge Description

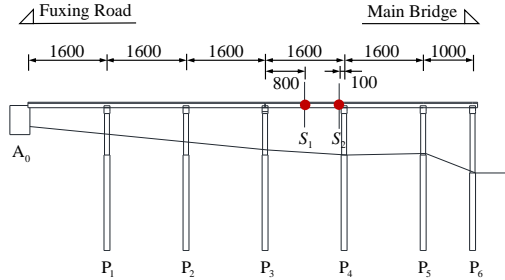
The instrumented concrete bridge (see Figure 4(a)) considered herein is a connection bridge located in the old section of Wanzhou District, Chongqing, China. It has the total length of 94.015 m, whose span composition is $5 \times 16 \text{ m} + 10 \text{ m}$ (see Figure 4(c)). The superstructure of this bridge consists of continuous hollow slab beams constructed of reinforced concrete. As shown in Figure 4(c), we name the bridge abutment A_0 and the piers $\{P_1, P_2, P_3, P_4, P_5, P_6\}$ orderly according to the vehicle moving direction to the main bridge. Two sections are monitored, marked as S_1 and S_2 in the mid-span of the fourth span and near the top of pier P_4 , respectively. Figure 4(d) shows that each monitoring section $S_i (i \in \{1, 2\})$ has five strain sensors installed on the bottom of the hollow slab beam. Vibrational chord strain gauges are installed which facilitate monitoring of both strain response of the bridge and the corresponding operation temperature (see Figure 4(b)).



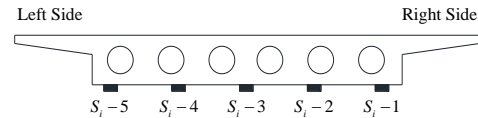
(a) Elevation view



(b) Vibrational chord strain gauge



(c) Monitoring sections of strain sensors



(d) Strain sensor locations at a typical section

Figure 4: The instrumented concrete bridge.

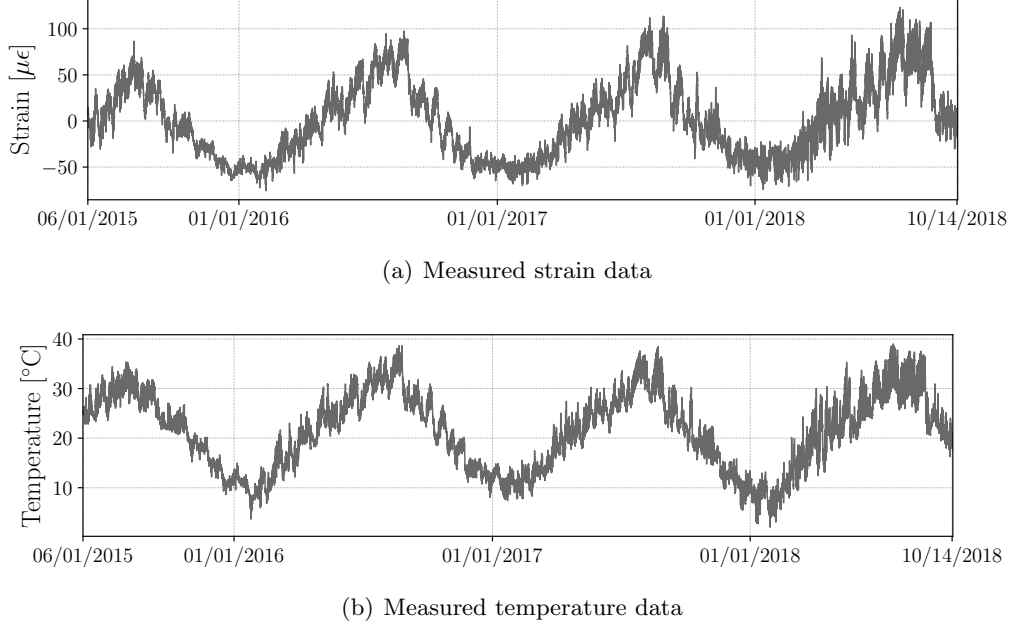


Figure 5: Time series of measurements at sensor S_{1-1}

The dataset collected from the above SHM system contains strain and temperature time histories recorded from June 1, 2015 to October 14, 2018. We resample the data at the rate of 10 min interval. Thus, it can be organized as a two-dimensional tensor with both strain data and temperature data (with a size of $20 \times 177,408$, representing sensors \times time stamps). The salient feature behind this data arrangement is that the tensor structure with both strain and temperature can capture a lower rank compared to the tensor structure with only strain data, due to the strong correlation between strain and temperature. Figure 5 illustrates the recorded strain and temperature time series for over three years from a typical sensor (e.g., S_{1-1} as shown in Figure 4(c) and 4(d)).

3.2. Scenarios of Missing Data

First of all, to evaluate the proposed model for imputation and forecasting, we only set data missing on the strain recordings while keeping the temperature data fixed/known. Here, the missing rate η (e.g., 20%) is introduced for the strain data in the validation experiments, which is computed as the ratio of the amount of missing data to the total amount of measurements. Secondly, to simulate the real-world missing conditions during monitoring period, we define three primary missing scenarios for the two-dimensional tensor data considered herein, following a similar experimental design procedure for higher-dimensional tensors discussed in [57]. The first scenario is called “random missing” which presents discrete and arbitrary lack of data in the time histories. Each strain entry in the data matrix is dropped randomly (e.g., following a uniform random distribution). The second scenario is termed as “structured missing” where there is data missing occurs continuously for certain periods (e.g., one day or consecutive days). It is a common scenario in practical SHM applications due to sensor malfunctioning, but more challenging and less investigated in literature. In particular, we structurally remove the strain data by selecting multiple days randomly and dropping the corresponding data to simulate a practical missing condition. The last scenario is named “mixed missing” which combines random missing and structured missing at different rates.

After setting the different missing scenarios, we define a sparse binary matrix $\mathbf{B} \in \mathbb{R}^{M \times T}$ ($b_{i,t} = 1$ if $(i, t) \in \Omega$ and 0 otherwise) to record the missing positions for the subsequent comparison be-

tween imputation results and the ground truth. The target dense tensor without data missing is named \mathbf{Y}_d , and the partially observed tensor \mathbf{Y} can be calculated element-wisely by $\mathbf{B} \odot \mathbf{Y}_d$, where \odot denotes the Hadamard product.

The imputation/forecasting accuracy ρ is defined as the root mean square error (RMSE) between the reconstructed/predicted data and the corresponding ground truth, normalized by the root mean square (RMS) of the target values:

$$\rho = \left(1 - \frac{\sqrt{\frac{1}{n} \sum_{i=1}^n (y_i - y_i^*)^2}}{\sqrt{\frac{1}{n} \sum_{i=1}^n y_i^2}} \right) \times 100\%. \quad (36)$$

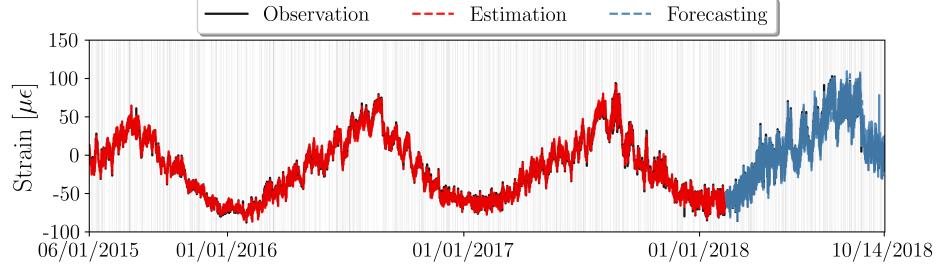
where y_i and y_i^* denote the ground truth and the estimated value at the same missing position i , and n is the total number of missing entries.

3.3. Results

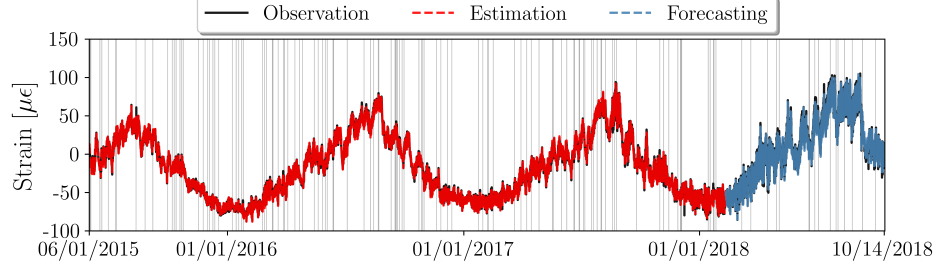
We test the overall performance of the proposed method and identify its limit of capacity for data imputation and response forecasting under various missing settings with different missing rates. The dataset is split into the first 80% segment (141,927 time instants) for imputation and the rest 20% data (35,481 points) for forecasting. To begin with, we first consider the missing rate of 10%, for both random and structured missing scenarios, while setting the tensor rank of eight. In addition, keeping the tensor rank fixed, we also set two mixed missing cases: Case 1 for 10% structured and 20% random missing occurring at the same time, while Case 2 for 20% structured and 30% random missing simultaneously. Here, sensor S₂₋₄ is selected to showcase the result. Figure 6 shows the corresponding imputation and forecasting result obtained by the proposed Bayesian tensor learning model. It can be seen that the predicted time series match well with the ground truth. In particular, the imputed data possess excellent agreement with the ground truth (see Figure 6(a) and (b)), while the forecasted response has relatively larger errors especially for the mixed missing cases with overall large missing rates (e.g., Case 1 and Case 2) as shown in Figure 6(c) and (d). In general, the spatiotemporal dependencies of the data are well learned by the proposed model. Besides, we provide a zoomed view of the predicted response by choosing one-week strain data (from December 1, 2017 to December 7, 2017) for the imputation test and another week strain time history (from August 8, 2018 to August 14, 2018) for the forecasting case (see Figure 7). It is notable that, despite large missing rates, the imputation is very robust and produces excellent estimation as shown in Figure 7(a), (c), (e) and (g). Though the forecasted responses exhibit noisy oscillations depicted in Figure 7(b), (d), (f) and (h), the overall trend is well captured (especially for relatively smaller missing rates, e.g., 10%).

To further investigate the performance of the proposed approach, we conduct uncertainty quantification of the prediction. The probabilistic imputation and forecasting results, with the mean and variance based on 100 Monte Carlo samples, are summarized in Figure 8. Specifically, Figure 8(a), (c), (e) and (g) show the imputed mean and two standard deviations of the strain response at Sensor S₂₋₄ in comparison with the ground truth record on March 7, 2018. The forecasted time series on August 9, 2018 for the same sensor are presented in Figure 8(b), (d), (f) and (h). For all these four missing scenarios, the imputation uncertainty is prominently smaller than the forecasting uncertainty. In the forecasting cases, it is observed that the missing data cause prediction fluctuations, which leads to deviation from the ground truth. Moreover, the forecasting uncertainty tends to be more unstable and larger when the missing rate becomes larger as shown in Figure 8(f) and (h).

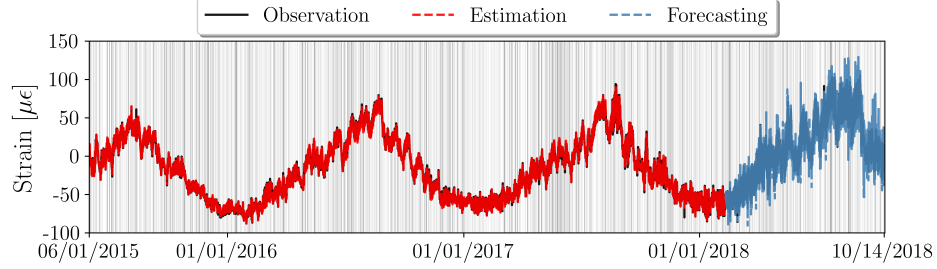
In addition, we perform parametric studies on the influence of data missing rate on the accuracy of imputation and forecasting. The test experiments arrange the first 80% portion of the recorded



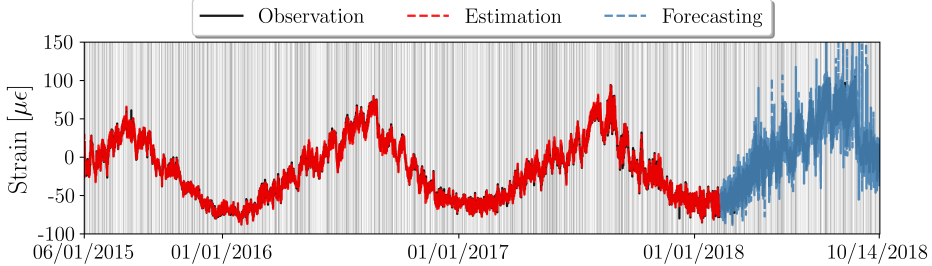
(a) Random missing scenario



(b) Structured missing scenario



(c) Mixed missing scenario (Case 1)



(d) Mixed missing scenario (Case 2)

Figure 6: The imputation and forecasting result for four missing cases at Sensor S_{2-4} . Note that the shading areas represent the time periods where data missing occurs, while the white box areas denote that the strain time series are successfully recorded. The dataset is split into the first 80% segment (in red color) for imputation and the rest 20% data (in blue color) for forecasting.

data for missing data recovery and the rest 20% for response forecasting. Figure 9 summarizes the parametric study result. For the random missing scenario shown in Figure 9(a), the proposed method presents outstanding accuracy (over 95% for both imputation and forecasting) given the missing rate η up to 70%. The extreme case we consider here is the missing condition with $\eta = 80\%$.

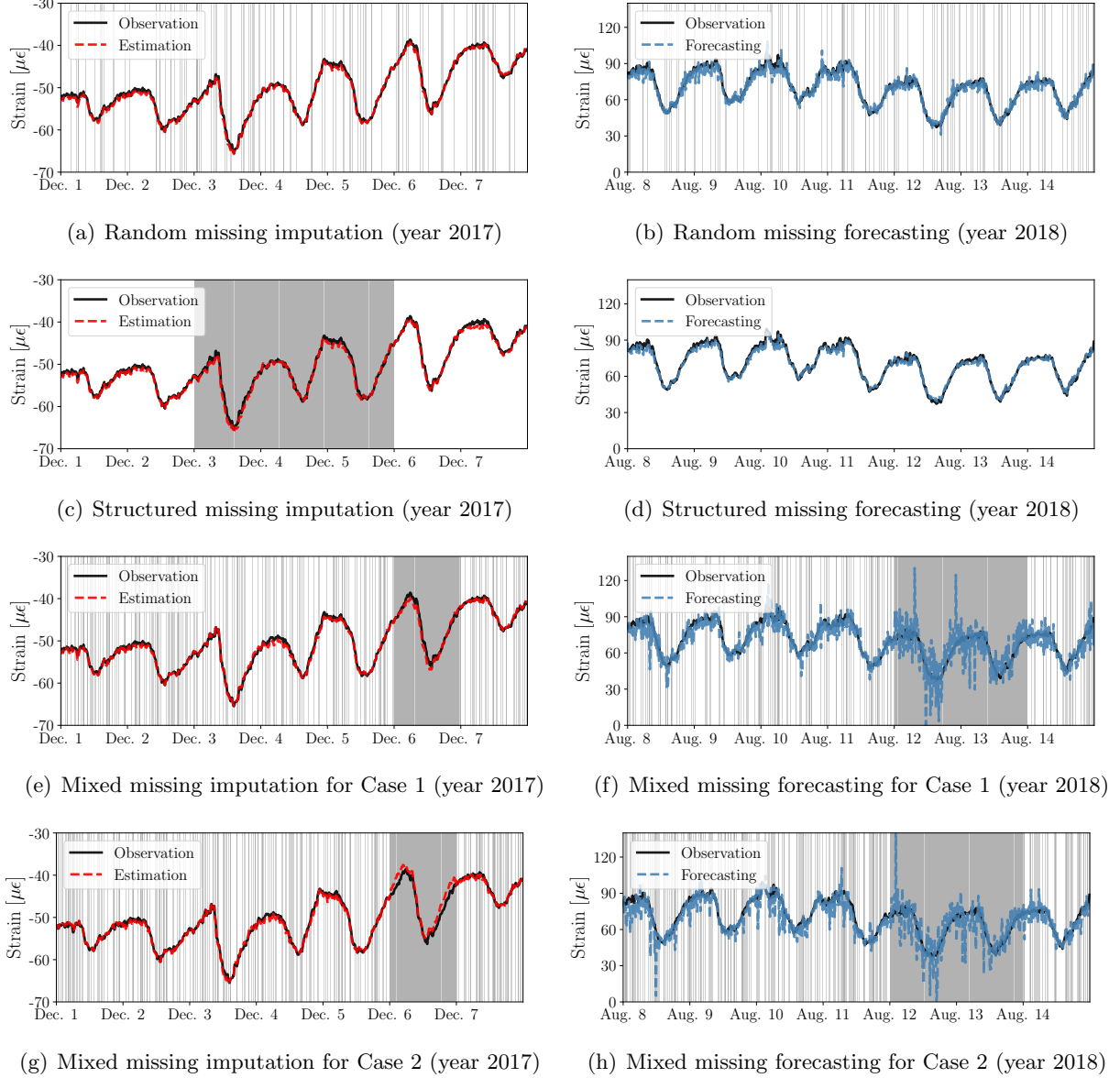
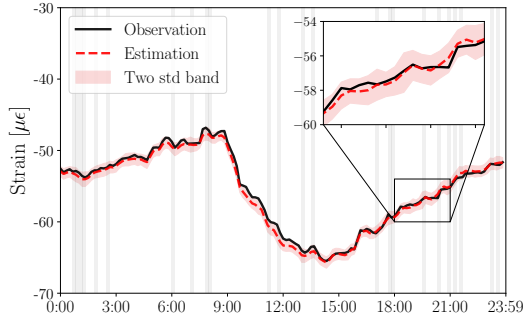
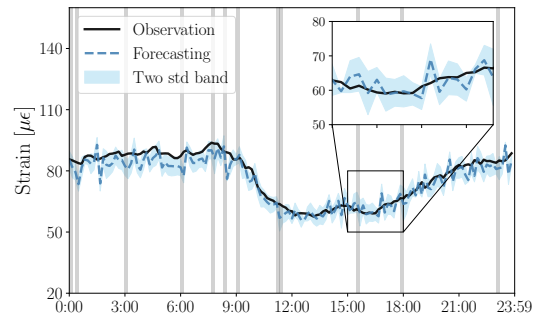


Figure 7: The zoomed view of the imputed and forecasted strain time series as shown in Figure 6. Note that the shading areas represent the time periods where data missing occurs, while the white box areas denote that the strain time series are successfully recorded.

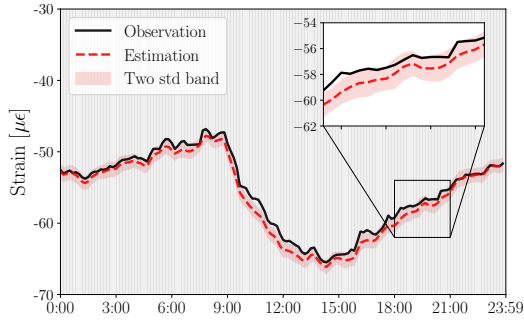
Nevertheless, the proposed approach still achieves over 86% missing data recovery accuracy and more than 92% forecasting accuracy. For the structured missing scenario (more practical and commonly seen in real-world applications), it is naturally more challenging to recover the missing data and forecast the response compared with the ideal random missing. As is seen in Figure 9(b), the capacity limit of the proposed Bayesian tensor learning method shows to be $\eta = 40\%$ where the imputation accuracy surpasses 91% while the forecasting has over 88% accuracy. Interestingly, the mixed missing scenarios demonstrate quite perfect imputation and forecasting accuracy, namely, 99.78% for imputation and 98.43% for forecasting in Case 1, and 99.59% for imputation and 97.18% for forecasting in Case 2. This result is closely related to optimal tensor rank selection which is discussed in Section 3.4.



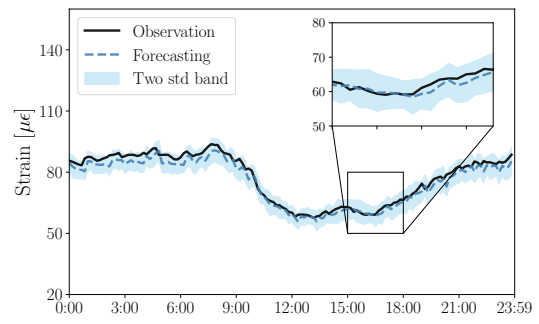
(a) Random Missing Imputation



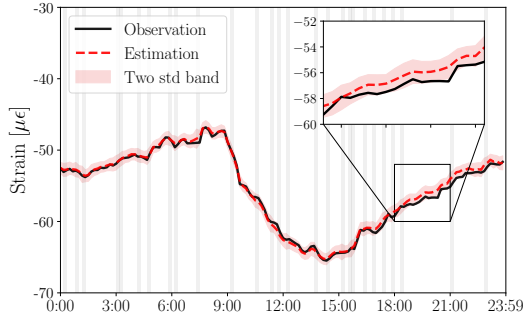
(b) Random Missing Forecasting



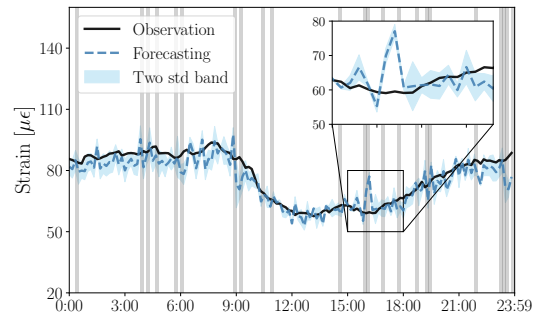
(c) Structured Missing Imputation



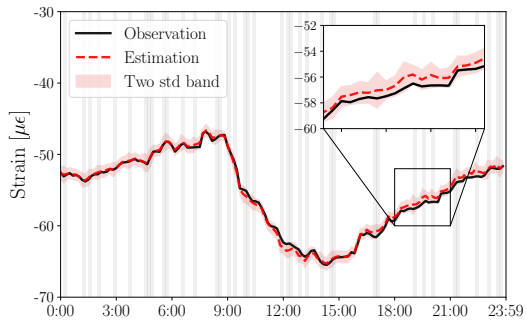
(d) Structured Missing Forecasting



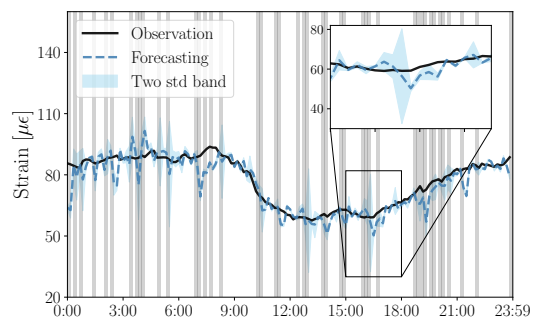
(e) Mixed Missing Imputation (Case 1)



(f) Mixed Missing Forecasting (Case 1)



(g) Mixed Missing Imputation (Case 2)



(h) Mixed Missing Forecasting (Case 2)

Figure 8: Uncertainty quantification of imputation and forecasting for four data missing cases.

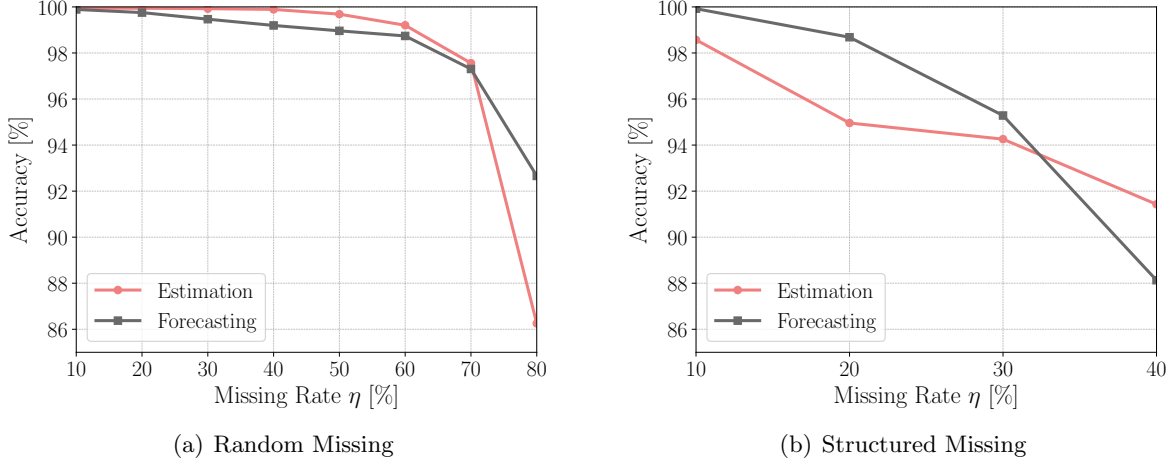


Figure 9: The accuracy of imputation and forecasting with respect to different data missing rates.

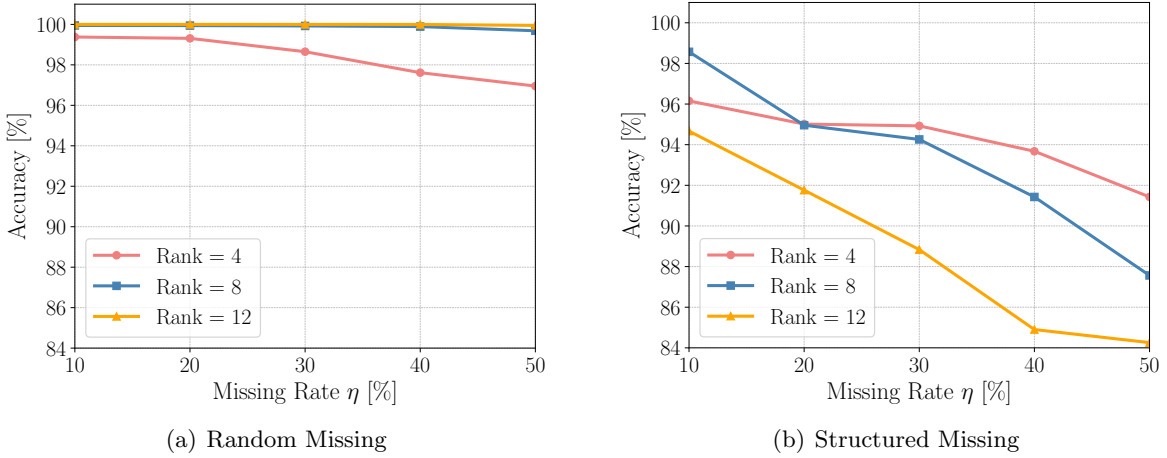


Figure 10: The performance imputation with respect to different tensor ranks.

3.4. Rank Analysis

There exist many recent researches attempting to reveal the effect of imperfect data on tensor representation [68–71]. According to [70], it is believed that clean datasets exhibit correlations across time and modalities while the imperfect data with incomplete values break these natural correlations and lead to the requirement of a higher rank. Inspired by this study, we also quantitatively investigate the prediction performance of the proposed Bayesian tensor learning method with different ranks (e.g., 4, 8 and 12) under different data missing scenarios (e.g., random and structured), and summarize the result in Figure 10. In particular, we test the imputation capability. As shown in Figure 10(a), with the increasing rank, the estimation achieves a better accuracy in the random missing scenario, which agree with the observation in [70]. In other words, random missing destroys the spatiotemporal correlations so that we should increase the tensor rank for a more accurate result when dealing with this type of imperfect data condition.

For the structured missing scenario (see Figure 10(b)), it is surprising to see that we get a higher accuracy of missing data recovery with a lower rank under different missing rates. We empirically extrapolate that continuous element missing helps to build a more correlated tensor structure.

4. Conclusions and Discussions

This paper presents a Bayesian tensor learning method for spatiotemporal data imputation and response forecasting for SHM applications, with the incorporation of the AR process which contributes to the temporal feature modeling. With the existence of temperature data, the tensor model can easily gain a low-rank structure and utilize the correlation between strain and temperature for robust prediction of the strain response. In our validation experiments, we both consider the ideal random missing scenario and a more realistic missing condition—structured missing. Based on the learned latent features, the accurate estimation and forecasting results show the satisfactory performance of the proposed approach for processing incomplete SHM recordings, with uncertainty quantification capability. In addition, the extreme cases illustrate that acceptable imputation and forecasting accuracy can retain for the missing rate up to $\eta = 80\%$ in random missing and up to $\eta = 40\%$ in structured missing. Furthermore, the investigation into rank selection has revealed that a lower rank helps achieve better prediction performance for structured missing, while a higher rank is preferred for random missing.

There are three highlights of the proposed method. The first and the most notable significance is that we model the temporal dependency via the latent features instead of using incomplete data directly, which offers a robust and flexible modeling scheme for multivariate time series data. Secondly, it is unnecessary to know which of the entries in the tensor data are incomplete beforehand. Thirdly, the fully Bayesian method can avoid overfitting and relax parameter tuning. In the meanwhile, it also draws unfavorable deficiency of computational complexity due to the use of approximated Bayesian inference. Notwithstanding the most time consuming process remains in the imputation process, this algorithm is efficient for response forecasting which can be potentially realized in real time.

The present study demonstrates that tensor learning has potential to become a promising area in SHM applications. Some future research directions and outlook are proposed herein. Firstly, as long as we have enough sensor locations and monitoring zones (e.g., distributed sensing), the higher order tensor decomposition for imputation and forecasting should be explored thanks to its possibility of outperforming the second-order tensor factorization [72]. Secondly, the proposed approach can be extended to tackle issues of SHM data anomaly detection and de-noising on account of the power of tensor representation. Last but not least, the spatial feature can be described in a more realistic way by considering graph kernels [51, 73], which will be worthy to investigate.

Acknowledgement

The authors would like to thank the Department of Bridge and Structural Engineering, China Merchants Chongqing Communications Technology Research and Design Institute Co. Ltd., for sharing the datasets which were used to validate the proposed methodology.

References

- [1] Y. Bao, H. Li, X. Sun, Y. Yu, J. Ou, Compressive sampling-based data loss recovery for wireless sensor networks used in civil structural health monitoring, *Structural Health Monitoring* 12 (1) (2013) 78–95.
- [2] Y. Bao, Y. Yu, H. Li, X. Mao, W. Jiao, Z. Zou, J. Ou, Compressive sensing-based lost data recovery of fast-moving wireless sensing for structural health monitoring, *Structural Control and Health Monitoring* 22 (3) (2015) 433–448.
- [3] Y. Huang, J. L. Beck, S. Wu, H. Li, Robust bayesian compressive sensing for signals in structural health monitoring, *Computer-Aided Civil and Infrastructure Engineering* 29 (3) (2014) 160–179.
- [4] Y. Bao, Z. Tang, H. Li, Compressive-sensing data reconstruction for structural health monitoring: a machine-learning approach, *Structural Health Monitoring* 19 (1) (2020) 293–304.

- [5] H. Cao, Y. Tian, J. Lei, X. Tan, D. Gao, F. Kopsaftopoulos, F. Chang, Deformation data recovery based on compressed sensing in bridge structural health monitoring, *Structural Health Monitoring* 2017 (shm).
- [6] K.-V. Yuen, H.-Q. Mu, A novel probabilistic method for robust parametric identification and outlier detection, *Probabilistic Engineering Mechanics* 30 (2012) 48–59.
- [7] K.-V. Yuen, G. A. Ortiz, Outlier detection and robust regression for correlated data, *Computer Methods in Applied Mechanics and Engineering* 313 (2017) 632–646.
- [8] H. Sun, O. Büyüköztürk, Bayesian model updating using incomplete modal data without mode matching, in: *Health Monitoring of Structural and Biological Systems 2016*, Vol. 9805, International Society for Optics and Photonics, 2016, p. 98050D.
- [9] I. Behmanesh, S. Yousefianmoghadam, A. Nozari, B. Moaveni, A. Stavridis, Effects of prediction error bias on model calibration and response prediction of a 10-story building, in: *Model Validation and Uncertainty Quantification*, Volume 3, Springer, 2016, pp. 279–291.
- [10] H. Sun, A. Mordret, G. A. Prieto, M. N. Toksöz, O. Büyüköztürk, Bayesian characterization of buildings using seismic interferometry on ambient vibrations, *Mechanical Systems and Signal Processing* 85 (2017) 468–486.
- [11] M. Song, I. Behmanesh, B. Moaveni, C. Papadimitriou, Modeling error estimation and response prediction of a 10-story building model through a hierarchical bayesian model updating framework, *Frontiers in Built Environment* 5 (2019) 7.
- [12] M. Song, I. Behmanesh, B. Moaveni, C. Papadimitriou, Hierarchical bayesian calibration and response prediction of a 10-story building model, in: *Model Validation and Uncertainty Quantification*, Volume 3, Springer, 2019, pp. 153–165.
- [13] M. Uzun, H. Sun, D. Smit, O. Büyüköztürk, Structural damage detection using bayesian inference and seismic interferometry, *Structural Control and Health Monitoring* 26 (11) (2019) e2445.
- [14] Z. Chen, R. Zhang, J. Zheng, H. Sun, Sparse bayesian learning for structural damage identification, *Mechanical Systems and Signal Processing* 140 (2020) 106689.
- [15] T. Yin, Q.-H. Jiang, K.-V. Yuen, Vibration-based damage detection for structural connections using incomplete modal data by bayesian approach and model reduction technique, *Engineering Structures* 132 (2017) 260–277.
- [16] L. D. Avendaño-Valencia, E. N. Chatzi, K. Y. Koo, J. M. Brownjohn, Gaussian process time-series models for structures under operational variability, *Frontiers in Built Environment* 3 (2017) 69.
- [17] L. D. Avendaño-Valencia, K. Tatis, E. N. Chatzi, Gaussian process vector ar surrogates for identification of structures under varying operational conditions, in: *Proceedings of the 8th Conference on Computational Stochastic Mechanics*, 2018, pp. 1–12.
- [18] L. D. Avendaño-Valencia, E. N. Chatzi, Modelling long-term vibration monitoring data with gaussian process time-series models, *IFAC-PapersOnLine* 52 (28) (2019) 26–31.
- [19] F. Kopsaftopoulos, S. Fassois, A functional model based statistical time series method for vibration based damage detection, localization, and magnitude estimation, *Mechanical Systems and Signal Processing* 39 (1-2) (2013) 143–161.
- [20] A. AMER, F. KOPSAPTOPOULOS, Probabilistic damage quantification via the integration of non-parametric time-series and gaussian process regression models, *Structural Health Monitoring* 2019.
- [21] H.-P. Wan, Y.-Q. Ni, Bayesian multi-task learning methodology for reconstruction of structural health monitoring data, *Structural Health Monitoring* 18 (4) (2019) 1282–1309.
- [22] Z. Chen, Y. Bao, H. Li, B. F. Spencer Jr, A novel distribution regression approach for data loss compensation in structural health monitoring, *Structural Health Monitoring* 17 (6) (2018) 1473–1490.
- [23] Y. Yang, S. Nagarajaiah, Harnessing data structure for recovery of randomly missing structural vibration responses time history: Sparse representation versus low-rank structure, *Mechanical Systems and Signal Processing* 74 (2016) 165–182.
- [24] Z. Chen, H. Li, Y. Bao, Analyzing and modeling inter-sensor relationships for strain monitoring data and missing data imputation: a copula and functional data-analytic approach, *Structural Health Monitoring* 18 (4) (2019) 1168–1188.
- [25] S.-C. Kuok, K.-V. Yuen, Model-free data reconstruction of structural response and excitation via sequential broad learning, *Mechanical Systems and Signal Processing* 141 (2020) 106738.
- [26] X. Fan, Bridge extreme stress prediction based on bayesian dynamic linear models and non-uniform sampling, *Structural health monitoring* 16 (3) (2017) 253–261.
- [27] J.-A. Goulet, Bayesian dynamic linear models for structural health monitoring, *Structural Control and Health Monitoring* 24 (12) (2017) e2035.
- [28] H. Wang, Y.-M. Zhang, J.-X. Mao, H.-P. Wan, T.-Y. Tao, Q.-X. Zhu, Modeling and forecasting of temperature-induced strain of a long-span bridge using an improved bayesian dynamic linear model, *Engineering Structures* 192 (2019) 220–232.
- [29] G. Park, D. J. Inman, Structural health monitoring using piezoelectric impedance measurements, *Philosophical Transactions of the Royal Society A: Mathematical, Physical and Engineering Sciences* 365 (1851) (2007) 373–

- [30] L. Bornn, C. R. Farrar, G. Park, K. Farinholt, Structural health monitoring with autoregressive support vector machines, *Journal of Vibration and Acoustics* 131 (2).
- [31] N. M. Okasha, D. M. Frangopol, D. Saydam, L. W. Salvino, Reliability analysis and damage detection in high-speed naval craft based on structural health monitoring data, *Structural Health Monitoring* 10 (4) (2011) 361–379.
- [32] H.-P. Wan, Y.-Q. Ni, Bayesian modeling approach for forecast of structural stress response using structural health monitoring data, *Journal of Structural Engineering* 144 (9) (2018) 04018130.
- [33] R.-T. Wu, M. R. Jahanshahi, Deep convolutional neural network for structural dynamic response estimation and system identification, *Journal of Engineering Mechanics* 145 (1) (2018) 04018125.
- [34] G. Fan, J. Li, H. Hao, Dynamic response reconstruction for structural health monitoring using densely connected convolutional networks, *Structural Health Monitoring* (2020) 1475921720916881.
- [35] R. Zhang, Y. Liu, H. Sun, Physics-guided convolutional neural network (PhyCNN) for data-driven seismic response modeling, *Engineering Structures* 215 (2020) 110704.
- [36] R. Zhang, Z. Chen, S. Chen, J. Zheng, O. Büyükoztürk, H. Sun, Deep long short-term memory networks for nonlinear structural seismic response prediction, *Computers & Structures* 220 (2019) 55–68.
- [37] R. Zhang, Y. Liu, H. Sun, Physics-informed multi-lstm networks for metamodeling of nonlinear structures, *arXiv preprint arXiv:2002.10253*.
- [38] C. Mylonas, I. Abdallah, E. Chatzi, Deep unsupervised learning for condition monitoring and prediction of high dimensional data with application on windfarm scada data, in: *Model Validation and Uncertainty Quantification, Volume 3*, Springer, 2020, pp. 189–196.
- [39] T. G. Kolda, B. W. Bader, Tensor decompositions and applications, *SIAM review* 51 (3) (2009) 455–500.
- [40] A. Anandkumar, R. Ge, D. Hsu, S. M. Kakade, M. Telgarsky, Tensor decompositions for learning latent variable models, *Journal of Machine Learning Research* 15 (2014) 2773–2832.
- [41] M. Janzamin, R. Ge, J. Kossaifi, A. Anandkumar, Spectral learning on matrices and tensors, *arXiv preprint arXiv:2004.07984*.
- [42] Q. Zhao, L. Zhang, A. Cichocki, Bayesian cp factorization of incomplete tensors with automatic rank determination, *IEEE transactions on pattern analysis and machine intelligence* 37 (9) (2015) 1751–1763.
- [43] L. Zhang, L. Zhang, D. Tao, X. Huang, B. Du, Compression of hyperspectral remote sensing images by tensor approach, *Neurocomputing* 147 (2015) 358–363.
- [44] C. Lu, J. Feng, Y. Chen, W. Liu, Z. Lin, S. Yan, Tensor robust principal component analysis: Exact recovery of corrupted low-rank tensors via convex optimization, in: *Proceedings of the IEEE conference on computer vision and pattern recognition*, 2016, pp. 5249–5257.
- [45] B. Du, M. Zhang, L. Zhang, R. Hu, D. Tao, Pltd: Patch-based low-rank tensor decomposition for hyperspectral images, *IEEE Transactions on Multimedia* 19 (1) (2016) 67–79.
- [46] X. Zhang, G. Wen, W. Dai, A tensor decomposition-based anomaly detection algorithm for hyperspectral image, *IEEE Transactions on Geoscience and Remote Sensing* 54 (10) (2016) 5801–5820.
- [47] Q. Shi, Y.-M. Cheung, Q. Zhao, H. Lu, Feature extraction for incomplete data via low-rank tensor decomposition with feature regularization, *IEEE transactions on neural networks and learning systems* 30 (6) (2018) 1803–1817.
- [48] A. Karatzoglou, X. Amatriain, L. Baltrunas, N. Oliver, Multiverse recommendation: n-dimensional tensor factorization for context-aware collaborative filtering, in: *Proceedings of the fourth ACM conference on Recommender systems*, 2010, pp. 79–86.
- [49] N. Ifada, R. Nayak, Tensor-based item recommendation using probabilistic ranking in social tagging systems, in: *Proceedings of the 23rd International Conference on World Wide Web*, 2014, pp. 805–810.
- [50] A. Seko, H. Hayashi, H. Kashima, I. Tanaka, Matrix-and tensor-based recommender systems for the discovery of currently unknown inorganic compounds, *Physical Review Materials* 2 (1) (2018) 013805.
- [51] H.-F. Yu, N. Rao, I. S. Dhillon, Temporal regularized matrix factorization for high-dimensional time series prediction, in: *Advances in neural information processing systems*, 2016, pp. 847–855.
- [52] H. Tan, G. Feng, J. Feng, W. Wang, Y.-J. Zhang, F. Li, A tensor-based method for missing traffic data completion, *Transportation Research Part C: Emerging Technologies* 28 (2013) 15–27.
- [53] M. T. Asif, N. Mitrovic, J. Dauwels, P. Jaillet, Matrix and tensor based methods for missing data estimation in large traffic networks, *IEEE Transactions on intelligent transportation systems* 17 (7) (2016) 1816–1825.
- [54] H. Tan, Y. Wu, B. Shen, P. J. Jin, B. Ran, Short-term traffic prediction based on dynamic tensor completion, *IEEE Transactions on Intelligent Transportation Systems* 17 (8) (2016) 2123–2133.
- [55] K. Takeuchi, H. Kashima, N. Ueda, Autoregressive tensor factorization for spatio-temporal predictions, in: *2017 IEEE International Conference on Data Mining (ICDM)*, IEEE, 2017, pp. 1105–1110.
- [56] D. Deng, C. Shahabi, U. Demiryurek, L. Zhu, R. Yu, Y. Liu, Latent space model for road networks to predict time-varying traffic, in: *Proceedings of the 22nd ACM SIGKDD International Conference on Knowledge Discovery and Data Mining*, 2016, pp. 1525–1534.

- [57] X. Chen, Z. He, J. Wang, Spatial-temporal traffic speed patterns discovery and incomplete data recovery via svd-combined tensor decomposition, *Transportation research part C: emerging technologies* 86 (2018) 59–77.
- [58] X. Chen, Z. He, L. Sun, A bayesian tensor decomposition approach for spatiotemporal traffic data imputation, *Transportation research part C: emerging technologies* 98 (2019) 73–84.
- [59] L. Sun, X. Chen, Bayesian temporal factorization for multidimensional time series prediction, *arXiv preprint arXiv:1910.06366*.
- [60] P. Rai, Y. Wang, S. Guo, G. Chen, D. Dunson, L. Carin, Scalable bayesian low-rank decomposition of incomplete multiway tensors, in: *International Conference on Machine Learning*, 2014, pp. 1800–1808.
- [61] Y. Xu, B. Chen, C. Ng, K. Wong, W. Chan, Monitoring temperature effect on a long suspension bridge, *Structural Control and Health Monitoring* 17 (6) (2010) 632–653.
- [62] Y.-F. Duan, Y. Li, Y.-Q. Xiang, Strain-temperature correlation analysis of a tied arch bridge using monitoring data, in: *2011 International Conference on Multimedia Technology*, IEEE, 2011, pp. 6025–6028.
- [63] Q. Xia, Y. Cheng, J. Zhang, F. Zhu, In-service condition assessment of a long-span suspension bridge using temperature-induced strain data, *Journal of Bridge Engineering* 22 (3) (2017) 04016124.
- [64] Y. Zhu, Y.-Q. Ni, A. Jesus, J. Liu, I. Laory, Thermal strain extraction methodologies for bridge structural condition assessment, *Smart Materials and Structures* 27 (10) (2018) 105051.
- [65] R. Salakhutdinov, A. Mnih, Bayesian probabilistic matrix factorization using markov chain monte carlo, in: *Proceedings of the 25th international conference on Machine learning*, 2008, pp. 880–887.
- [66] C. Andrieu, A. Doucet, R. Holenstein, Particle markov chain monte carlo methods, *Journal of the Royal Statistical Society: Series B (Statistical Methodology)* 72 (3) (2010) 269–342.
- [67] W. R. Gilks, P. Wild, Adaptive rejection sampling for gibbs sampling, *Journal of the Royal Statistical Society: Series C (Applied Statistics)* 41 (2) (1992) 337–348.
- [68] H. Fan, Y. Chen, Y. Guo, H. Zhang, G. Kuang, Hyperspectral image restoration using low-rank tensor recovery, *IEEE Journal of Selected Topics in Applied Earth Observations and Remote Sensing* 10 (10) (2017) 4589–4604.
- [69] X. Chen, Z. Han, Y. Wang, Q. Zhao, D. Meng, L. Lin, Y. Tang, A general model for robust tensor factorization with unknown noise, *arXiv preprint arXiv:1705.06755*.
- [70] P. P. Liang, Z. Liu, Y.-H. H. Tsai, Q. Zhao, R. Salakhutdinov, L.-P. Morency, Learning representations from imperfect time series data via tensor rank regularization, *arXiv preprint arXiv:1907.01011*.
- [71] Y. Chang, L. Yan, X.-L. Zhao, H. Fang, Z. Zhang, S. Zhong, Weighted low-rank tensor recovery for hyperspectral image restoration, *IEEE Transactions on Cybernetics*.
- [72] B. Ran, H. Tan, Y. Wu, P. J. Jin, Tensor based missing traffic data completion with spatial–temporal correlation, *Physica A: Statistical Mechanics and its Applications* 446 (2016) 54–63.
- [73] M. T. Bahadori, Q. R. Yu, Y. Liu, Fast multivariate spatio-temporal analysis via low rank tensor learning, in: *Advances in neural information processing systems*, 2014, pp. 3491–3499.